energies

Article

Irradiation Analysis of Tensile Membrane Structures for Building-Integrated Photovoltaics

Janusz Marchwiński [1], Vuk Milošević [2], Anna Stefańska [3] and Elena Lucchi [4,*]

1 Faculty of Architecture, University of Ecology and Management in Warsaw, 00-792 Warsaw, Poland; j.marchwinski@wseiz.pl
2 Faculty of Civil Engineering and Architecture, University of Niš, 18000 Niš, Serbia; vukamer@yahoo.com
3 Institute of Civil Engineering, Warsaw University of Life Sciences, 02-787 Warsaw, Poland; anna_stefanska@sggw.edu.pl
4 Department of Architecture, Built Environment and Construction Engineering (DABC), Politecnico di Milano, 20133 Milan, Italy
* Correspondence: elena.lucchi@polimi.it

Abstract: A dynamic development in building-integrated photovoltaics (BIPVs) has been observed in recent years. One of the manifestations of this trend is the integration of photovoltaic cells with tensile membrane structures, including canopies. Such solutions bring mutual benefits—the roofs provide a potentially large area for the application of photovoltaic cells while contributing to the improvement of the energy efficiency of the building. However, what is lacking is thorough research on the most favourable photovoltaic cell exposure within these roofs. This paper investigates the optimal position of photovoltaic cells in terms of energy gains related to exposure to solar radiation. Hypar geometries were simulated as the most characteristic of tensile membrane roofs and, simultaneously, the least obvious in the research context. Simulations were performed for 54 roof samples with the following geometric variables: roof height (1.0, 3.0 m) and membrane prestress (1:3, 1:1, 3:1). The research was conducted for three roof orientations defined by azimuth angles of 0, 22.5, and 45 degrees and three geographic locations, Oslo, Vienna, and Lisbon, representing Northern, Central, and Southern Europe, respectively. The Sofistik and Rhino + Ladybug software were used to create models and simulations. The study results show significant differences in the roof irradiation and, consequently, the optimal location of BIPVs depending on the above variables. Generally, it is the curvature that is the most important variable-less curved roofs are more irradiated and thus more suitable for BIPVs. Prestress and the azimuth angle are of lesser significance, but defining the optimal use of a BIPV depends on the adopted scenario regarding the percentage of membrane coverage with PVs—other recommendations concern the strategy of total or partial roof coverage with PV cells. The difference between optimally and incorrectly designed roofs may amount to a 50% electricity gain from PV cells.

Keywords: BIPVs; tensile membrane structures; membrane roofs; energy efficiency; photovoltaic technology

check for updates

Citation: Marchwiński, J.; Milošević, V.; Stefańska, A.; Lucchi, E. Irradiation Analysis of Tensile Membrane Structures for Building-Integrated Photovoltaics. *Energies* **2023**, *16*, 5945. https://doi.org/10.3390/en16165945

Academic Editor: Alon Kuperman

Received: 20 July 2023
Revised: 30 July 2023
Accepted: 9 August 2023
Published: 11 August 2023

1. Introduction

Energy production from renewable energy sources (RESs) [1–3] is essential to address the energy dependency of European countries on other nations [4], both for new and existing buildings. The European legislative framework calls for the widespread application of RESs to tackle energy dependency and climate change, aiming to reduce energy needs, environmental emissions, and economic costs [5]. Furthermore, the implementation of RESs can lead to human comfort, security, well-being, and social engagement and stimulate economic growth, investments, and property values [6,7]. Among RES options, photovoltaic (PV) systems show significant promise due to continuous improvements in PV cell designs and performance, along with their reliability [8,9], versatility [9], and scalability [9,10]. Otherwise, unlike other solar technologies, such as solar thermal (ST) and hybrid systems

(PVTs), they support the energy transition towards supply-side strategies, guarantying on-site production [10,11], self-consumption coverage [9,10], and energy peak shaving [9]. Promoting energy autarky [12], "*users*" transform into energy-independent "*producers*", receiving remuneration for energy production and selling to the national energy grid [1]. Hence, they are also "*prosumers*", a term combining "*producers*" and "*consumers*".

PV systems can be applied directly to buildings in two primary ways: building-attached PVs (BAPVs) and building-integrated PVs (BIPVs). In the first case, PV modules are mounted on the building envelope with mechanical elements that can be easily removed [13]. In contrast, BIPVs involve replacing conventional building elements with PV materials, creating a construction product with both energy and building functions [13–16]. It is important to note that dismantling BIPV products requires replacing the entire building element [14].

Despite a high potential from an environmental standpoint, PVs face various constraints and uncertainties. The constraints mainly involve applications in sensitive areas, where limitations mainly concern the PV cell's aesthetic appearance and the system's reversibility [8]. Additionally, policy [17–21], economic [17–19,22], information [18,19], human resource [7,18,23], and technical [17] issues have been identified as hindrances. The complexity of the legislative framework [17–21] and the economic costs of PV systems [17–19,22] are recognised as the industry's main problems. Moreover, technical stakeholders' insufficient knowledge of innovative approaches is a particular concern, especially in undeveloped countries [7,18,23]. Technical uncertainties revolve around the energy and aesthetic performance of innovative PV cells [10], as well as life-cycle assessment (LCA) and the sustainability of the manufacturing process [7,11]. Critiques have also arisen regarding the difficulties in integrating rigid PV systems into building envelopes because the structures need high mechanical resistance to sustain these systems [24]. This limitation confines the application of rigid PVs mainly to roofs, curtain walls, and regular façades, reducing electric production because of shading in high-density cities and lowering irradiation on vertical elements [24]. In this context, PV textile membranes offer new possibilities by integrating PV modules into the textile structure via sewing or bonding [25]. PV membranes allow for tailored aesthetic designs thanks to the flexibility and adaptability of their shapes, geometries, colours, and patterns. As a result, this technology holds significant potential for the building sector. The background of flexible PV systems depends mainly on solar cells and substrates. Hence, a detailed overview of flexible PVs is provided to understand the state of the art in product innovation and research applications related to this topic. In this context, this paper aims to assess the feasibility of PV tensile membrane structures across various climatic conditions. It seeks to demonstrate the impact of irradiation on different building shapes and orientations when integrating such structures.

2. Background on Flexible PV

PV technology's aesthetic appearance, technical quality, and energy performance have improved drastically in the last twenty years. The first generation of PV solar cells (SCs) was based mainly on silicon wafers (e.g., monocrystalline, polycrystalline, amorphous, or hybrid silicon cells), low-iron glass-cover sheets, and encapsulants. Monocrystalline and polycrystalline cells are the most frequently used thanks to their higher energy efficiency (19–25%), longer-lasting duration, and reduced costs [26]. Their aesthetic appearance is not appealing because of the presence of blue colours, square shapes, and high thicknesses. Other drawbacks are the absence of flexibility, low geometrical adaptability, and reduced efficiency with high environmental temperatures (>25 °C). Conversely, amorphous cells have improved flexibility thanks to the adaptation of curved subphases, manufacturing cost reductions, and better performance with low light levels. The disadvantages are low energy efficiency (≅10%) and complex production methods that hinder their architectonical application. Thus, hybrid silicon cells try to combine the advantages of crystalline and amorphous silicon cells. The second generation of PV cells is composed mainly of thin films made by low-thickness semiconductors composed of amorphous silicon and nonsilicon materials, such as cadmium–telluride and copper indium gallium diselenide. Their advantage is a cost reduction due to eliminating silicon wafers, higher dimensions, and improved energy efficiency (15–20%) [26]. The most recent innovation in PVs refers to the third generation, which is composed of several materials, including dye-sensitised (DSSCs), copper–zinc tin sulphide (CZTS), quantum dot (QDSCs), perovskite (PSCs), and organic PV (OPV) solar cells. They have very different energy, technical, and aesthetic performances because of their physical–chemical structures. For example, DSSCs use synthetic dyes to replace chlorophyll in plants to reproduce a photosynthesis scheme [27]. They have high flexibility in shape, colour, and transparency; low cost; and an environmentally friendly manufacturing process [27], but on the other hand, they have low energy efficiency (≅7.1%) and high environmental sensitivity (liquid electrolytes may freeze or evaporate at low or high temperatures). CZTSs and QDSCs are less exploited because of complicated fabrication processes, relatively low energy efficiency (CZTs ≅ 13% and QDSCs ≅ 10%), high costs [25,27], and the presence of toxic elements (such as the presence of particle sizes that are hard to control) [28]. PSCs are structured compounds composed of organic and inorganic materials (e.g., methylammonium lead halides, inorganic caesium lead halides, and tin-halide-based materials) [28]. They have high flexibility, a low cost, a high power-to-weight ratio (≅19.5%), and involve facile fabrication techniques but, conversely, reduced mechanical robustness, low long-term stability (particularly relative humidity, which can generate degradation issues), high-efficiency drops, and high manufacturing costs [25,29]. Finally, OPVs have environmentally friendly manufacturing processes, low weight (especially ultrathin OPVs), high mechanical performance, and geometrical flexibility [25,27]. The disadvantages are decay risks at high temperatures, low energy efficiency (≅10%), and performance instability over the passage of time [25].

Flexible PVs encompass the second and third generations of PV materials [24]. Both PSCs and OPVs can be integrated into PV textile membranes, which benefit from their flexibility and easy production techniques, similar to textile processes, and this has created new markets for PV applications [29]. The flexibility of solar cells mainly depends on the substrates used. They can be divided into [25] (i) plastic and (ii) metallic substrates. Plastic ones are composed of polymeric materials (e.g., PEN, PET, PTFE, ETFE). These substrates are characterised by low cost, high optical transparency, chemical stability, and favourable bendability [25]. However, they have certain disadvantages, including high deformation, reduced mechanical resistance, and limited tolerance to high temperatures [25,30]. Metallic ones are manufactured using copper or stainless-steel foils. These substrates offer advantages like good thermal stability, high corrosion resistance, and charge conductivity. However, they are less transparent, resulting in their opacity being a drawback [25].

After the first studies referring to the chemical composition of PV cells for improving their performance [24], studies on the design and calculation of PV performance arose. Early studies investigated the compatibility between PV designs and advanced parametric models to research the technical, aesthetic, and energy possibilities of tailored BIPV tensile membrane structures [27]. The most widely used parametric tool is the Grasshopper parametric plug-in for Rhino, known for its ability to optimise multiple environmental parameters [24]. Concurrently, numerical simulation software such as ANSYS, EASY, and ABAQUS is employed for structural designs [24]. For instance, Zanelli et al. [31] developed a prototype for integrating ethylene-tetra-fluorine-ethylene (ETFE) with OPVs. They discussed the fabricating approach, the printing techniques, and the pattern possibilities thanks to the support of Grasshopper. Ibrahim et al. [32] assessed the PV layout and daylighting patterns of a BIPV tensile membrane using the Grasshopper software. This method predicted structural performance and payback time under different mechanical and environmental conditions. An important topic is related to form-finding processes to optimise the shape of PV tensile membrane structures using dynamic relaxation [33], finite element [34], and force density [35], methods. Dynamic structural analyses are preferred for understanding the structural feasibility of the curved shapes of inflatable membrane structures [35].

Our literature review shows the following key findings:

- PV tensile membrane structures are an emergent field of research, defying proper definitions [25] and studies on this technology's state-of-the-art [24].
- This technology's development and manufacturing are improving continuously, mainly focusing on chemical and physical characteristics [25,29].
- The thermal, electrical, structural, and aesthetic performance of PV tensile membranes integrated with buildings has rarely been developed [27].
- PV tensile membrane structures need a customised project, different from conventional PV products that are also realised in mass-customisation applications [24,27].

Indeed, given the complex challenges and the potential of PV tensile membrane structures, there is a clear need for optimisation studies that encompass various aspects such as geometrical design, structural integrity, energy efficiency, and electrical performance. These studies should be conducted under different climatic conditions to gain insights into how irradiation affects different building shapes and orientations. By conducting such comprehensive optimisation studies, it is possible to better understand and harness the potential of PV tensile membrane structures, paving the way for the more efficient and effective integration of PV tensile membranes in the built environment.

3. Materials and Methods

This study uses numerical models to explore the influence of different parameters on the insolation of PV tensile membranes and, consequentially, the production of electric energy. To this end, the research methodology is structured into the following parts:

- Primary model definition (Section 3.1) using the finite elements and form-finding technique to precisely define its geometry.
- Parameter variation (Section 3.2) for describing the parameters that will be varied to check their influence on the results.
- Results (Section 4) on the influence of the variation of different parameters on the energy efficiency of the PV tensile membrane design.
- Discussion (Section 5) of the recommendations for optimising the energy efficiency of the PV tensile membrane.
- Conclusion (Section 6) highlighting the pros, cons, and challenges of the irradiation analysis of BIPV tensile membrane structures.

3.1. Preliminary Model Definition

In the first step, a single model of a membrane structure needed to be defined. The model represents the most common and basic membrane geometry, a hyperbolic paraboloid (hypar). As explained in a later section, we decided to run the research with the use of two separate programs. The numerical model of tensile membranes was first obtained in the software Sofistik [36]. This is a finite element software used for analyses of various types of structures. In this research, it was used to obtain the geometry of the membrane under defined structural parameters, using the modified force density method. Thanks to this software, it was possible to explore differences in geometry under various membrane prestress ratios. Final irradiation models were investigated in Rhinoceros/Grasshopper, using the Ladybug plug-in. The Ladybug software was essential for the calculations thanks to the possibility of using exact energy data from chosen locations. Obtained geometries were analysed in terms of location and orientation.

The hypar models are commonly used in scientific research. Regardless of the material, whether rigid reinforced concrete or lightweight membranes, these surfaces help minimise the material through moment-free performance. The development of saddle geometries was evident in design practice during initial form-finding studies, including in the canopies of Frei Otto and Felix Candela. Gosling et al. [37] defined a simple hypar model of a tensile structure later used in other studies [38]. This is a four-point membrane with cable edges. The decision to alter this model with respect to the edge properties was made. Compared with the flexible cable edges of the proposed model, in this research, rigid and straight membrane edges were used. The reason for this adjustment was the presumption that, to obtain larger areas covered by the PV, these membranes will be multiplied and connected, and this is much easier and more reasonable to accomplish with membranes with straight edges. At the same time, membranes with straight edges individually allow for a somewhat larger area to be covered. Finally, the preliminary test model is defined with properties that are provided in Table 1, while the visual representation of the preliminary test model is provided in Figure 1.

Table 1. Properties of the preliminary model of a tensile membrane structure (source: authors' elaboration).

Type	Dimension
Base (m)	6 × 6
Height (m)	1
Warp prestress (kN/m)	3
Weft prestress (kN/m)	3
Membrane edges (-)	Rigid, straight
Warp direction (-)	Diagonal
Membrane warp modulus (kN/m)	600
Membrane weft modulus (kN/m)	600
Membrane shear modulus (kN/m)	30
Membrane Poisson's ratio (-)	0.4

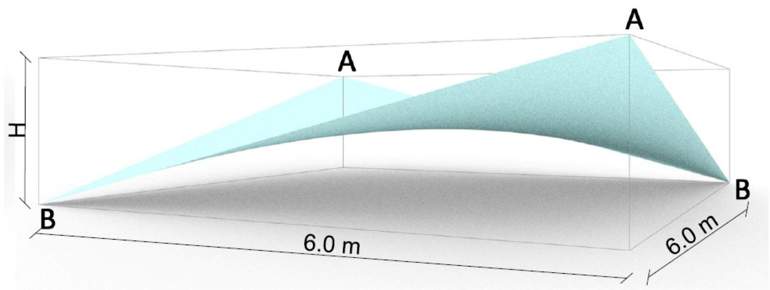

Figure 1. The preliminary model (source: elaboration by the authors).

3.2. Parameter Validation

This research aims to explore the impact of parameters that affect the insolation of the membrane and, consequentially, their influence on the production of electrical energy. Therefore, four variable parameters were introduced to provide information about the relationship between the parameter and the PV efficiency. For this purpose, the following variable parameters were chosen for the irradiation analysis:

- The curvature of the membrane (its total height).
- Prestress ratio of the membrane.
- Orientation of the structure.
- Geographic location of the structure.

The first variable parameter is the membrane curvature, which varies significantly. Thus, it is expected to impact the installed PV system considerably. With the size of the base fixed, the largest changes in curvature can be obtained by altering the height of the structure. Therefore, we decided to make two alterations to the preliminary model regarding the height (H) of the model. Tensile membrane structures require the curvature to be stable, so it was not reasonable to use a height of 0 m (H0). A height of 1 m (H1) was selected as the lower one and a height of 3 m (H3) as the higher one, providing two values for this variable suitable for analysing the trends among the produced results. The changes in the form of the model using this parameter are shown in Figure 2.

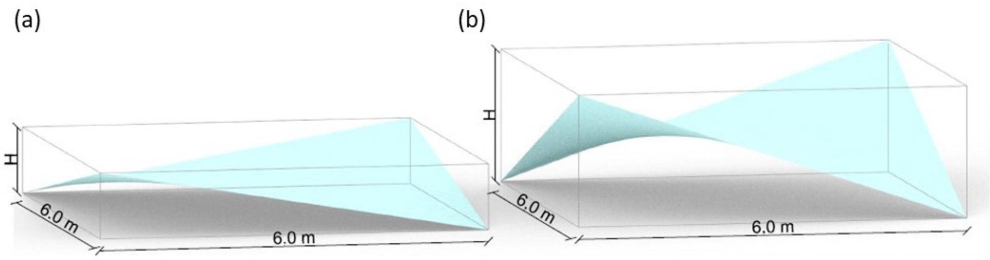

Figure 2. The form of models with different heights: (**a**) model with a total height of 1 m (H1), (**b**) model with a total height of 3 m (H3) (source: elaboration by the authors).

Another way to subtly change the model's curvature is by changing the prestress ratio. The prestress of the preliminary test model was taken to be equal in the warp and weft directions. This is frequently the case in tensile membranes. However, different prestress ratios are sometimes defined for several reasons. One of the most common is the change in the structure's shape that occurs as a result. It is worth mentioning that the proportional change in the prestress value does not reflect the change in the membrane form since the form remains unaltered. From a structural point of view, uneven prestress intensities make sense when the expected loading on the structure is larger in one of the vertical directions or when the material properties are not equal in the two principal directions. Because of this, prestress ratios of 3:1 and 1:3 in the warp-to-weft direction were added to the research, next to a 1:1 prestress ratio for the first test model. The geometrical models were prepared to obtain the correct geometry under different prestress ratios. Model shape changes were less visible than with the previous parameter. Hence, the differences in the structures' side views, with the marked middle point of each structure, are shown in Figure 3.

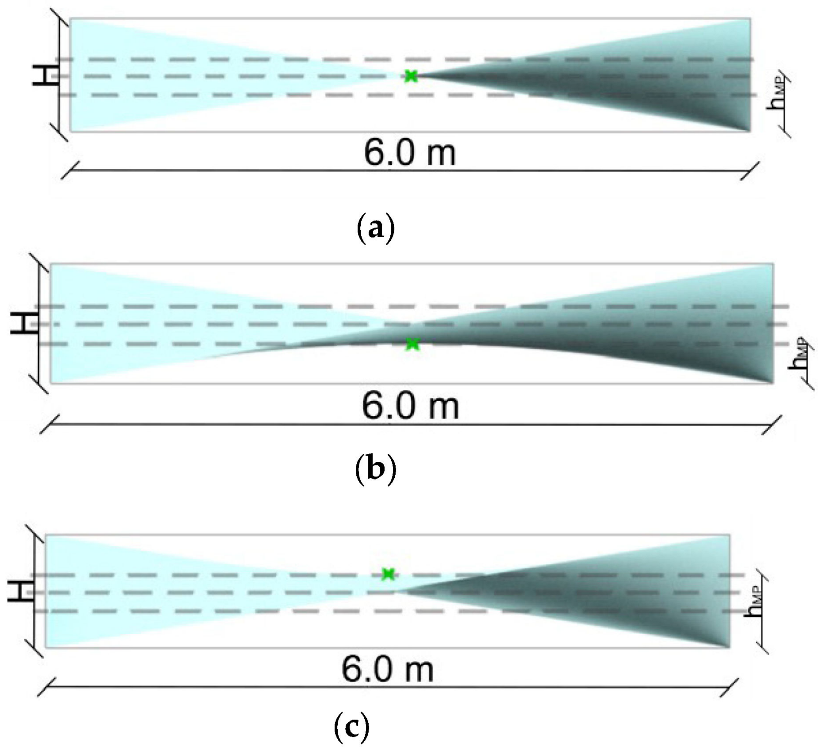

Figure 3. The shape under different prestress ratios; the green point represents the middle point of each membrane (height of the middle point: h_{MP}): (**a**) prestress 1:1, (**b**) prestress 1:3, (**c**) prestress 3:1 (source: elaboration by the authors).

Orientation may have a significant influence on final energy production [27]. Exemplary measurements of energy gains from PVs for different orientations of building envelopes (roofs, façades) are included in [39], showing significant differences in gains depending on these variables. Thus, orientation is the third varied parameter. This parameter is not closely related to the visual or structural properties but can rather impact the insolation of the structure. It should be noted that the analysed models are both radially symmetric from the centre of the structure and axially symmetric across its diagonals. Therefore, rotating the structure by 180 degrees does not change its geometry and insolation. The initial tests proved that rotation by 90 degrees does not affect the insolation of the membrane either. Hence, three values were selected for this study, 0° orientation, 22.5° orientation, and 45° orientation, with the rotation defined as the angle between the horizontal projection of the first membrane edge and the north, as presented in Figure 4.

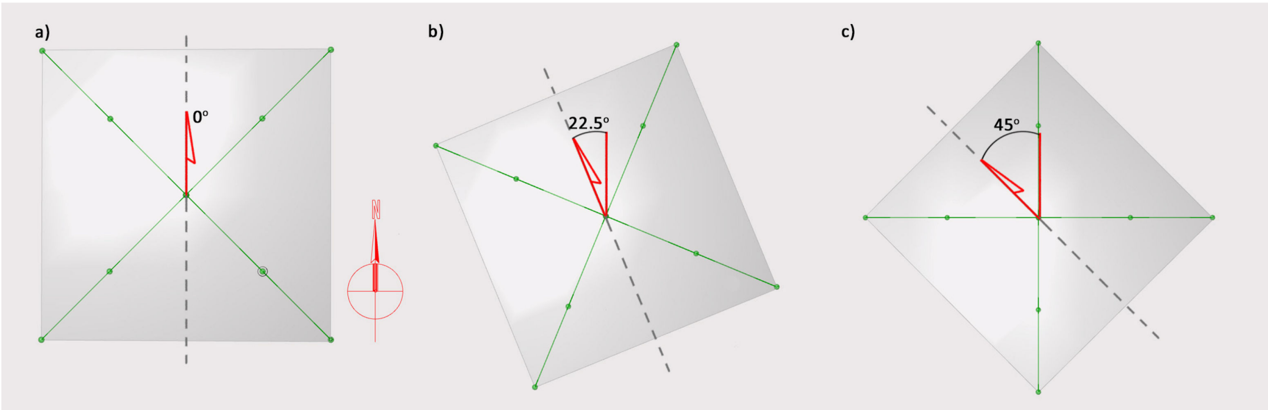

Figure 4. The orientation of the structure: (**a**) rotation by 0°, (**b**) rotation by 22.5°, (**c**) rotation by 45° (source: elaboration by the authors).

The geographic location of the model is usually not set by the designer of the structure but is instead already provided to him. However, how this parameter influences other selected parameters and their relationship with the PV system is unclear. It is the goal of this research to clarify this issue. For this reason, three different locations were selected for the models. All three are within Europe and capital cities, representing the continent's northern, central, and southern parts. The selected locations were Oslo, Vienna, and Lisbon. The different latitudes of the locations provided the results needed to analyse the effects of this parameter and its influence on other parameters. The locations and their exact environmental parameters were based on the Ladybug weather file sources, an online tool for the Ladybug Grasshopper analysis software (www.ladybug.tools/epwmap/, accessed on 13 July 2023) [40]. The crucial parameter was the yearly average irradiance value measured for the horizontal surface, which amounted to ca. 950 kWh/m^2, 1200 kWh/m^2, and 1700 kWh/m^2 for Oslo, Vienna, and Lisbon, respectively. A visual representation of the available locations and the annual average solar irradiation selected for the research cities are shown on the map in Figure 5.

An overview of the values of all the varied parameters is provided in Table 2. A combination of all the values of the variable parameters provided the number of analysed models. The total number of studied models was, therefore, 54.

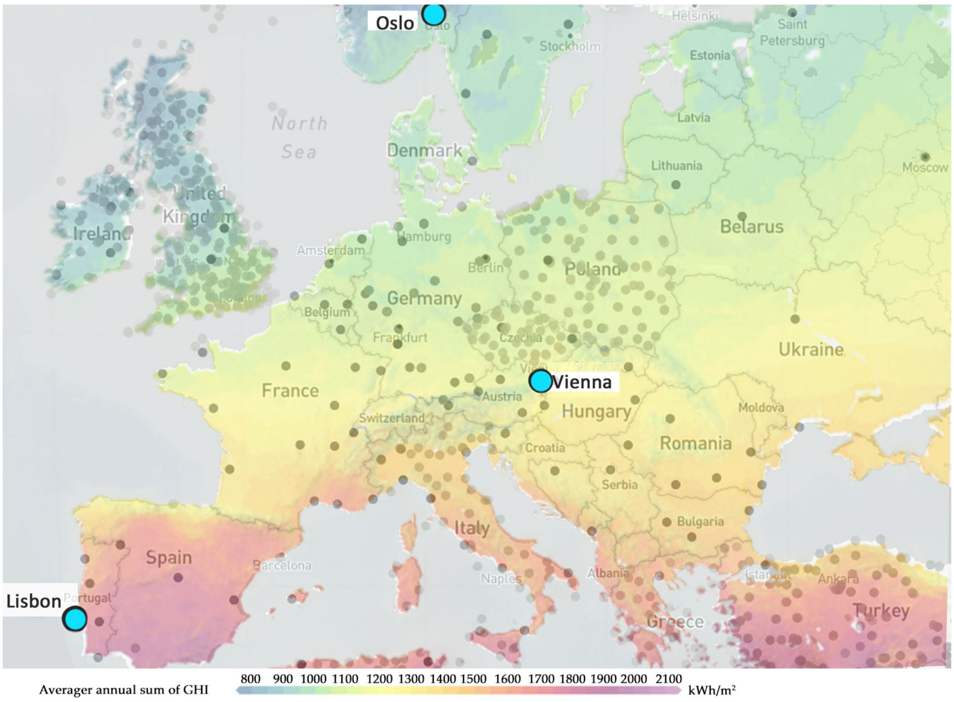

Figure 5. The geographic location of the structure (source: elaboration by the authors).

Table 2. Overview of the analysed parameters (source: elaboration by the authors).

Analysed Parameter	Analysed Values		
Height (m)	1	3	
Membrane prestress ratio	1:3	1:1	3:1
Orientation (°)	0	22.5	45
Geographic location	Oslo	Vienna	Lisbon

3.3. Insolation and PV System

To study the optimal position of the PV system on the membrane, a straightforward methodology was created to examine different parts of the membrane. Nine points were selected on the membrane surface as reference points. These points were positioned along the diagonals of the model. Diagonal A contains two high supports, and diagonal B contains two low supports. The position of the selected points is presented in Figure 6.

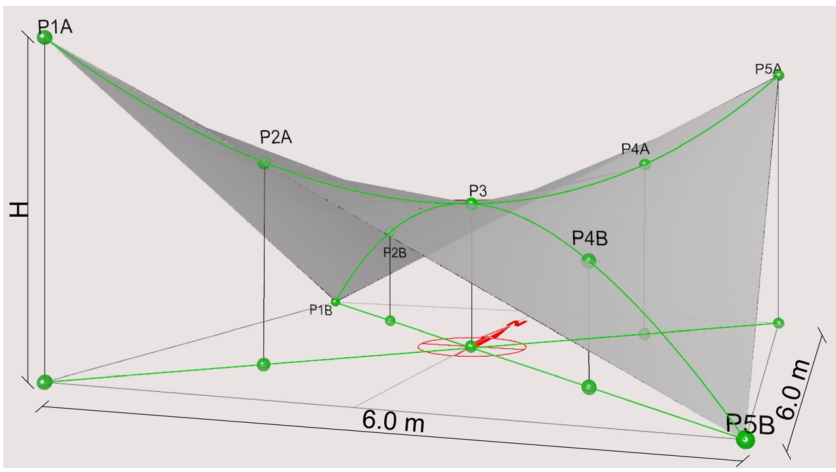

Figure 6. Position of the selected points on the model (source: elaboration by the authors).

The higher supports are marked as points P1A and P5A, while the lower supports are marked as P1B and P5B. Point P3 is located at the centre of the membrane, where the diagonals intersect. Point P2A is positioned in the middle between P1A and P3; point P2B is at half the distance between P1B and P3. The rest of the points are arranged symmetrically. The purpose of this was to check the total annual irradiation on these points to conclude at which position the PV system will be optimally exploited. Despite the symmetry of the models, it is expected that the symmetrical points will not be equally irradiated because of the curvature of the membrane and the elevation of the sun. These positions were carefully arranged to cover the surface of the membrane evenly and ensure sufficient data for analysis.

4. Results

According to the research assumptions (Section 3), the results of the roof insolation measurements in the tested variants are presented in two ways:

- A general measurement of the average insolation of the roofs, broken down into the percentage share of insolation in four accepted ranges of values (Section 4.1).
- Insolation measurements at characteristic points of the roof (Section 4.2).

4.1. Distribution of Irradiation on the Whole Surface of Membrane Roofs

Because of the irregular, complex shape of the membrane roofs, the distribution of insolation on their surfaces was first examined based on the adopted variables (Figure 7).

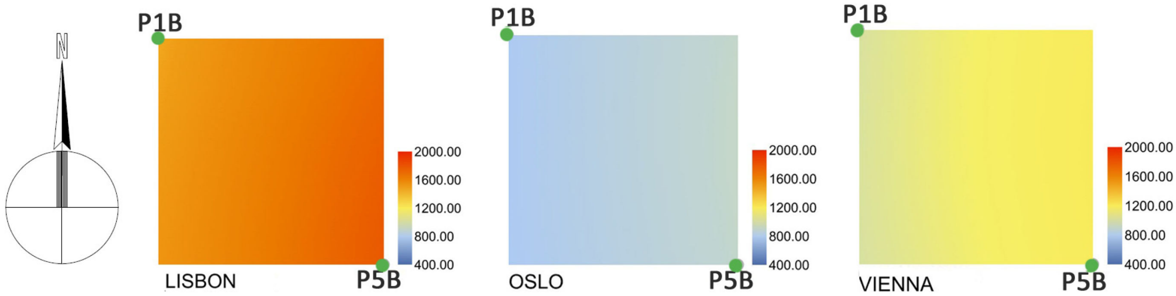

Figure 7. The preliminary model irradiation map plans for Lisbon, Oslo, and Vienna (from left)—differentiated tints reflect irradiance values according to the columns beside them (in kWh/m^{2}a) measured on an irregular hypar roof surface (source: elaboration by the authors).

This distribution is shown based on the conventional division into four ranges of insolation values:

- 400–800 kWh/m^{2}a, representing low insolation values (average values typical for extreme northern regions of Europe).
- 800–1200 kWh/m^{2}a, representing moderate insolation values (average values for northcentral European areas).
- 1200–1600 kWh/m^{2}a, representing high insolation values (average values for the regions of Central and Southern Europe).
- 1600–2000 kWh/m^{2}a, representing the highest insolation values (average values for the extreme southern areas of Europe).

The average insolation values for the tested variants were also calculated. The results are included in Figure 8.

	height	prestress
variant	1	1:1

OSLO				VIENNA				LISBON			
[kWh/m2]	0.0°	22.5°	45.0°	[kWh/m2]	0.0°	22.5°	45.0°	[kWh/m2]	0.0°	22.5°	45.0°
400-800	9.88	9.47	9.81	400-800	0.00	*99.62*	0.00	400-800	0.00	0.00	0.00
800-1200	90.12	*90.53*	90.19	800-1200	100	0.38	98.52	800-1200	0.00	0.00	0.00
1200-1600	0.00	0.00	0.00	1200-1600	0.00	0.00	1.47	1200-1600	42.06	42.11	41.78
1600-2000	0.00	0.00	0.00	1600-2000	0.00	0.00	0.00	1600-2000	57.94	57.89	*58.22*
Σ	100	100	100	Σ	100	100	100	Σ	100	100	100
average	868.58	868.55	868.53	average	1107.82	1107.87	1107.88	average	1617.24	1617.5	1617.57

variant	3	1/1

OSLO				VIENNA				LISBON			
[kWh/m2]	0.0°	22.5°	45.0°	[kWh/m2]	0.0°	22.5°	45.0°	[kWh/m2]	0.0°	22.5°	45.0°
400-800	40.62	41.06	41.30	400-800	0.48	3.34	4.24	400-800	0.00	0.00	0.00
800-1200	*59.38*	58.94	58.70	800-1200	*84.62*	79.56	78.26	800-1200	6.68	6.88	7.92
1200-1600	0.00	0.00	0.00	1200-1600	14.90	17.10	17,5	1200-1600	46.5	45.62	47.14
1600-2000	0.00	0.00	0.00	1600-2000	0.00	0.00	0.00	1600-2000	46.82	*47.5*	44.94
Σ	100	100	100	Σ	100	100	100	Σ	100	100	100
average	830.44	830.58	830.91	average	1053.99	1054.53	1054.75	average	1542.69	1545.10	1545.79

variant	1	1/3

OSLO				VIENNA				LISBON			
[kWh/m2]	0.0°	22.5°	45.0°	[kWh/m2]	0.0°	22.5°	45.0°	[kWh/m2]	0.0°	22.5°	45.0°
400-800	16.86	23.22	24.54	400-800	0.00	0.00	0.00	400-800	0.00	0.00	0.00
800-1200	*83.14*	76.78	75.46	800-1200	*100*	94.92	89.56	800-1200	0.00	0.00	0.00
1200-1600	0.00	0.00	0.00	1200-1600	0	5.08	10.44	1200-1600	44.33	45.38	45.90
1600-2000	0.00	0.00	0.00	1600-2000	0.00	0.00	0.00	1600-2000	*55.67*	54.62	54.10
Σ	100	100	100	Σ	100	100	100	Σ	100	100	100
average	865.86	865.84	865.81	average	1104.48	1104.51	1104.51	average	1612.20	1612.25	1612.25

variant	3	1/3

OSLO				VIENNA				LISBON			
[kWh/m2]	0.0°	22.5°	45.0°	[kWh/m2]	0.0°	22.5°	45.0°	[kWh/m2]	0.0°	22.5°	45.0°
400-800	46.09	46.47	46.46	400-800	4.93	15.95	18.00	400-800	0.00	0.00	0.00
800-1200	*53.91*	53.53	53.54	800-1200	*88.72*	56.71	52.94	800-1200	3.07	19.77	23.51
1200-1600	0.00	0.00	0.00	1200-1600	6.35	27.34	29.06	1200-1600	*53.71*	33.54	29.00
1600-2000	0.00	0.00	0.00	1600-2000	0.00	0.00	0.00	1600-2000	43.22	46.69	47.49
Σ	100	100	100	Σ	100	100	100	Σ	100	100	100
average	811.34	810.83	810.57	average	1030.29	1030.50	1030.54	average	1506.85	1507.00	1507.54

variant	H1	3:1

OSLO				VIENNA				LISBON			
[kWh/m2]	0.0°	22.5°	45.0°	[kWh/m2]	0.0°	22.5°	45.0°	[kWh/m2]	0.0°	22.5°	45.0°
400-800	13.53	2.06	1.73	400-800	0.00	0.00	0.00	400-800	0.00	0.00	0.00
800-1200	86.47	97.94	*98.27*	800-1200	*100*	99.97	99.95	800-1200	0.00	0.00	0.00
1200-1600	0.00	0.00	0.00	1200-1600	0.00	0.03	0.05	1200-1600	43.89	42.58	39.73
1600-2000	0.00	0.00	0.00	1600-2000	0.00	0.00	0.00	1600-2000	56.11	57.42	*60.27*
Σ	100	100	100	Σ	100	100	100	Σ	100	100	100
average	868.35	868.30	868.30	average	1107.18	1107.28	1107.34	average	1616.70	1617.43	1617.67

variant	H3	3:1

OSLO				VIENNA				LISBON			
[kWh/m2]	0.0°	22.5°	45.0°	[kWh/m2]	0.0°	22.5°	45.0°	[kWh/m2]	0.0°	22.5°	45.0°
400-800	41.33	38.82	38.58	400-800	1.96	0.20	0.28	400-800	0.00	0.00	0.00
800-1200	58.67	61.18	*61.42*	800-1200	85.48	93.15	*93.81*	800-1200	17.02	1.80	1.04
1200-1600	0.00	0.00	0.00	1200-1600	12.56	6.65	5.91	1200-1600	33.25	49.06	62.07
1600-2000	0.00	0.00	0.00	1600-2000	0.00	0.00	0.00	1600-2000	49.73	49.14	36.89
Σ	100	100	100	Σ	100	100	100	Σ	100	100	100
average	829.29	829.36	829.55	average	1049.14	1050.52	1051.26	average	1537.80	1544.14	1545.97

Figure 8. Percentage distribution of irradiation values in four selected value ranges. Note: orange fields = the highest percentage value in the highest range of irradiation; yellow fields = the highest percentage value in the lowest range of irradiation; green text: the highest average value of irradiation; red text = the highest percentage value regardless of the value range of irradiation (source: elaboration by the authors).

The measured results allow for the formulation of basic observations:

- As expected, there is considerable variation in insolation depending on the geographical location.
- The measured values for Oslo fall within the first two ranges, with a predominance in a range of 800–1200 kWh/m^{2}a. However, there are large differences in insolation in both ranges depending on the roof geometry (e.g., for the higher range: 90.53% for height = 1 and prestress 1:1; 53.91% for height = 3 and prestress 1:3).
- Generally, Oslo's range of values is smaller than the other locations.
- The values for Vienna additionally cover a range of 1200–1600 kWh/m^{2}a. Depending on the geometrical variables of the roof, the share of insolation is the most diverse in the highest range measured for Vienna (0.05% for height = 1, prestress 3:1, azimuth 45°; 29.06% for height 3, prestress 1:3, azimuth 45°). The largest percentage is in the medium range: 800–1200 kWh/m^{2}a.
- The values measured for Lisbon also cover the three ranges studied, but they are mainly in the higher ranges, i.e., over 1200 kWh/m^{2}a. The highest share of insolation falls on the highest range, i.e., >1600 kWh/m^{2}a.
- The average insolation of roofs for Lisbon is about 1.8–1.9 times the insolation value for Oslo and about 1.5 for Vienna.
- Differences between the average insolation values for a given location are the smallest depending on the azimuthal angle and the largest for the prestress variable. This applies to all locations.
- Depending on the geometrical variables of the roof, the highest percentages of the best and worst sunlit surfaces occur in the case of Oslo at all azimuth angles tested.
- For Vienna, the highest and lowest shares are generally only for the angles of 0° and 45°. One exception occurs: the largest share of the worst insolation area (in the lowest range) was measured only once for the angle of 22.5°, i.e., for height 1, prestress 1/1.
- In the case of Lisbon, the situation is similar, with the difference that the exception is the extreme percentage result, not for the worst but for the best sunlit surfaces (in the highest range of insolation) for the angle of 22.5°. It was measured for a height of 3 m and a prestress of 1:1.
- It is also characteristic that Oslo has no azimuthal angles for which the highest and lowest percentages of insolation could be measured simultaneously among measurements of the same roof geometry (same height and prestress).
- In the cases of Vienna and Oslo, this happens at both 0° and 45°.

4.2. Irradiation Values at Characteristic Points of Membrane Roofs

Insolation measurements were made at selected points within two diagonals of the membrane roof projection on a square plan:

- Diagonal A: Concave geometry with the lower vertices of the roof at points P1A and P5A, in common with the second diagonal, the midpoint (neutral) P3, and the points located at an equal distance between P1A–P3A and P1A–P5A (i.e., points P2A and P4A, respectively).
- Diagonal B: Convex geometry with the top vertices of the roof at points P1A and P5B, the midpoint (neutral) P3, and the points located equidistant between P1B–P3B and P1B–P5B (i.e., points P2B and P4B, respectively).

Measurements were made for all variables: roof height, prestress azimuth, and geographical location. The selected points were considered characteristic (i.e., representative of individual parts of the membrane roof). The measurement points are reported below (Figure 9).

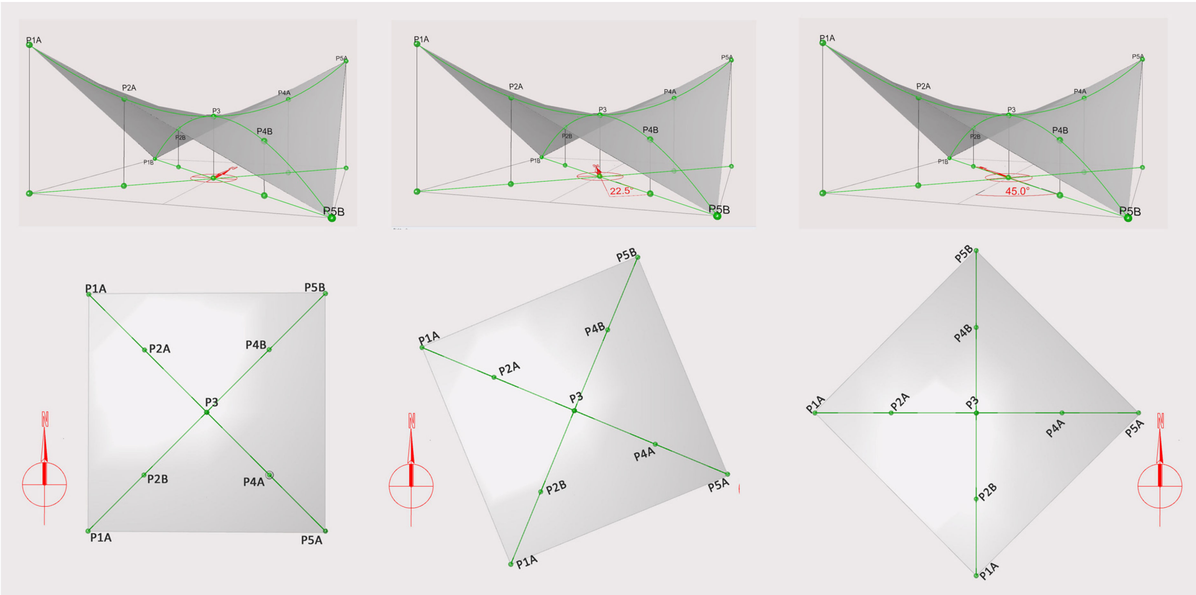

Figure 9. Measurement points on roof geometries (layout and axonometry) in three variants of the azimuth angle (source: elaboration by the authors).

The results are included in the following figures for all conditions. Model 1 considers all the locations (Lisbon, Vienna, Oslo), all orientations (azimuth 0°, 22.5°, and 45°), a height of 1 m (H1), and a prestress ratio of 1:1 (Figure 10).

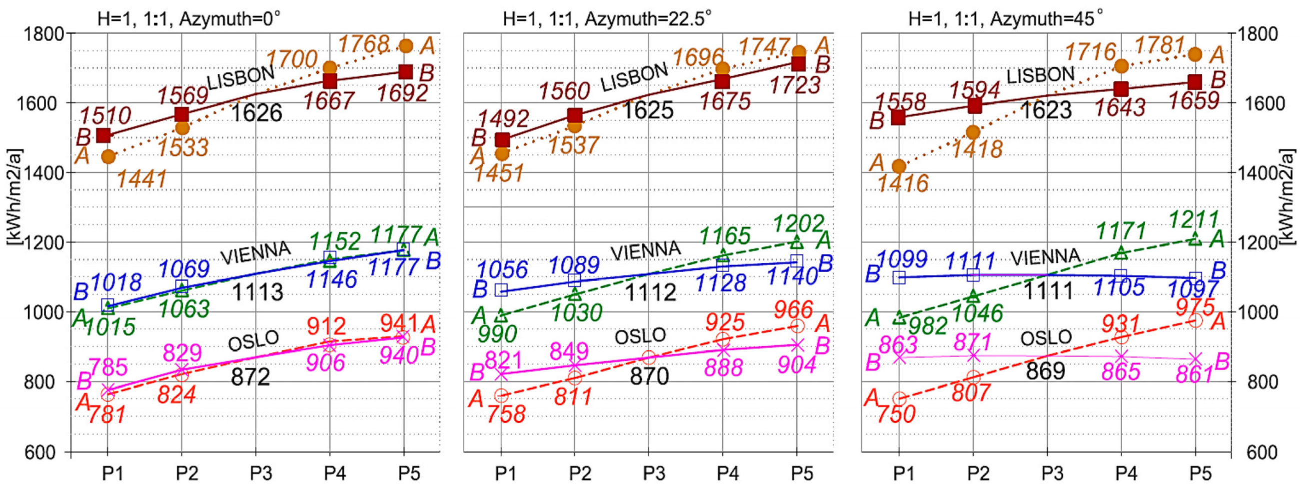

Figure 10. Model 1: Irradiation values for five points on two diagonals (A and B) measured for all locations, all orientations, a height of 1 m (H = 1), and a prestress ratio of 1:1 (source: elaboration by the authors).

Model 2 changes the height of Model 1 from 1 m to 3 m (H3) and maintains all other parameters (Figure 11).

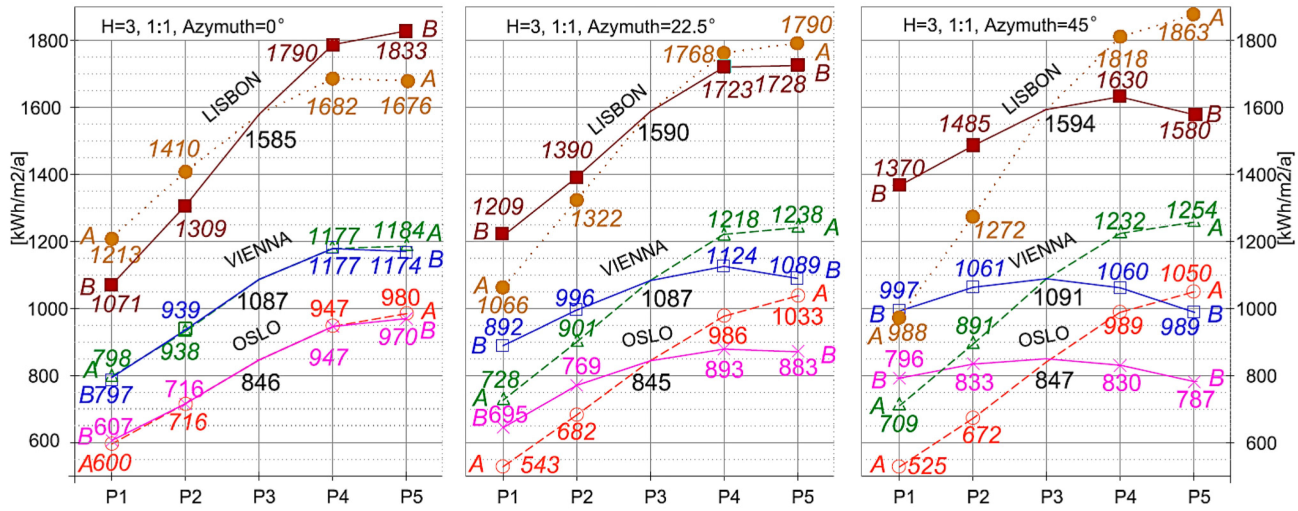

Figure 11. Model 2: Irradiation values for five points on two diagonals (A and B) measured for all locations, all orientations, a height of 3 m (H = 3), and a prestress ratio of 1:1 (source: elaboration by the authors).

Model 3 changes the prestress ratio of Model 1 from 1:1 to 1:3 and maintains all the other parameters (Figure 12).

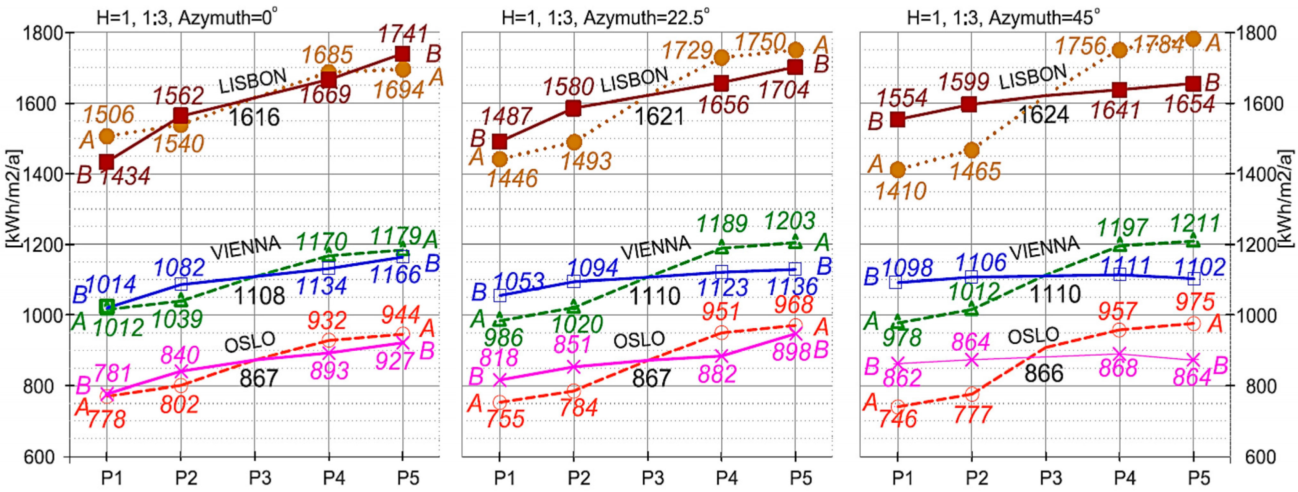

Figure 12. Model 3: Irradiation values for five points on two diagonals (A and B) measured for all locations, all orientations, a height of 1 m (H = 1), and a prestress ratio of 1:3 (source: elaboration by the authors).

Model 4 changes the height of Model 3 from 1 m to 3 m (H3) and maintains all the other parameters (Figure 13).

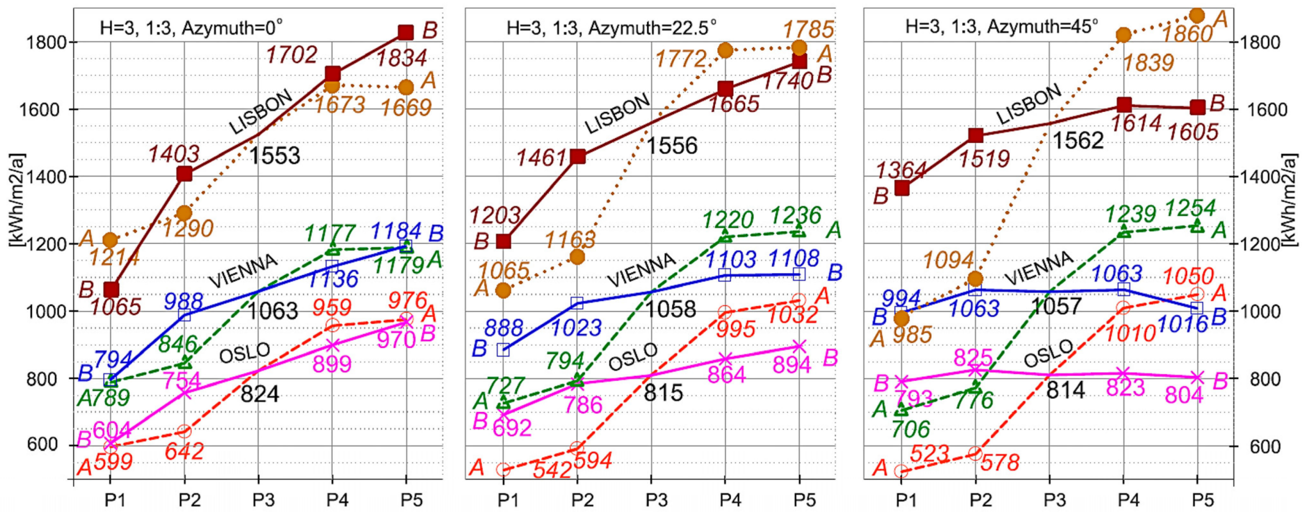

Figure 13. Model 4: Irradiation values for five points on two diagonals (A and B) measured for all locations, all orientations, a height of 3 m (H = 3), and a prestress ratio of 1:3 (source: elaboration by the authors).

Model 5 changes the prestress ratio of Model 1 from 1:3 to 3:3 and maintains all the other parameters (Figure 14).

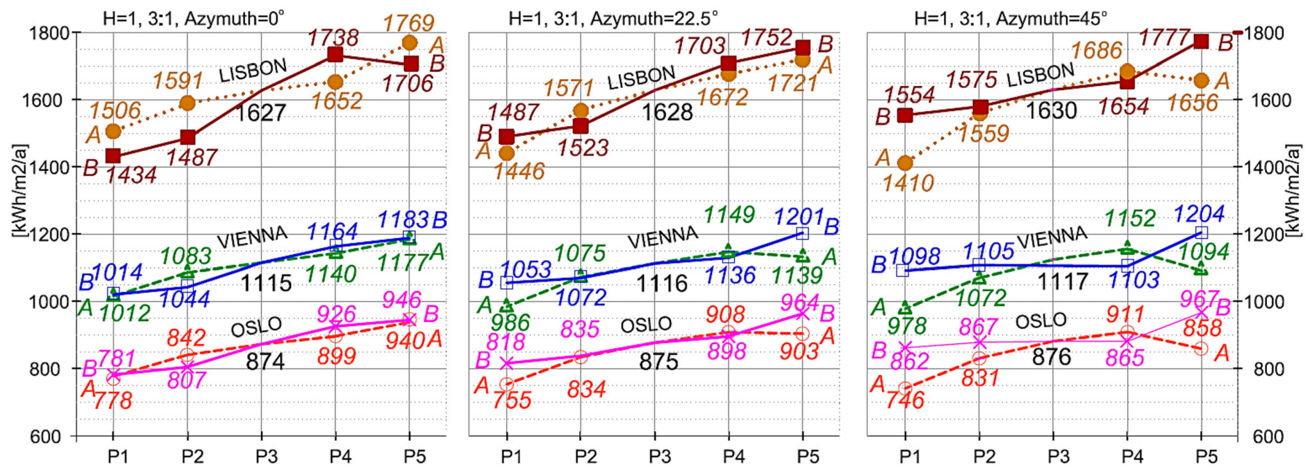

Figure 14. Model 5: Irradiation values for five points on two diagonals (A and B) measured for all locations, all orientations, a height of 1 m (H = 1), and a prestress ratio of 3:1 (source: elaboration by the authors).

Model 6 changes the height of Model 5 from 1 m to 3 m (H3) and maintains all the other parameters (Figure 15).

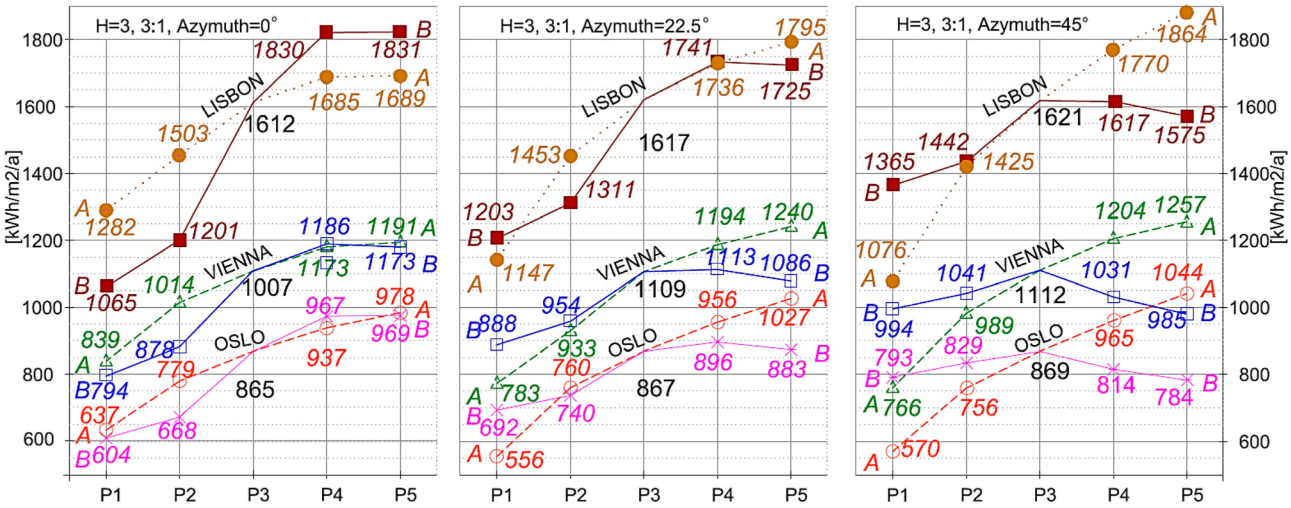

Figure 15. Model 6: Irradiation values for five points on two diagonals (A and B) measured for all locations, all orientations, a height of 3 m (H = 3), and a prestress ratio of 3:1 (source: elaboration by the authors).

The measured results allow the following basic regularities to be observed:

- Areas around points P4–P5 generally receive more sunlight than those around P1 and P2.
- The difference is greater in the points on diagonal A (concave line). In this case, the difference is more significant with a higher roof height. It increases with the increase in the roof height (the graphs are steeper for H = 3 than H = 1).
- In diagonal B, the differences decrease with the increase in the azimuth angle, and in some cases for the angle of 45° (Oslo and Vienna at H = 3 and H = 1, prestress 1:1), the surfaces at points 1B-2B are better exposed to sunlight, although the differences are minor (compared with P1A–2A).
- The highest insolation values were generally measured at the P5A points, i.e., points located in the convex upper area of the membrane roof on the sunny side (although there is an exception for H = 1.3:1, angle 45°, and for the same geometry at 22.5° for Oslo and Vienna, where the highest value is at point P4A).
- The values at the bottom concave peak, P5B, are lower than P5A. Point P5B in the tested cases is always the best sunlit point on diagonal B only for the azimuthal angle of 0 degrees. For an angle of 22.5°, it loses its leading position in some variants to point P4 (e.g., H = 3, prestress 3:1), while in the case of an angle of 45°, the insolation value at P5B is usually no longer the highest, and once even becomes the smallest among the other values of points on axis B (H = 3, 1:1; Oslo and Vienna). This is because the slope on which the P3–P5 diagonal lies is most exposed to the south.
- In turn, the least insolated peaks are P1A, i.e., opposite to the most insolated ones—the differences between P1A and P1B increase with the increase in the azimuthal angle.
- A comparison of irradiation values between corresponding points on the A and B diagonals indicates that the differences are generally more visible between the extreme points and decrease towards the central part of the roof plan. However, this applies to symmetrical roofs (prestress 1:1). The results are more varied for prestresses 1:3 and 3:1. In many cases, the most significant differences occur between the intermediate points, P2 and P4. Still, the general regularity, noticeable in the case of prestress 1:1, cannot be observed (this aspect is discussed in more detail in Section 5).
- The graphs for Oslo and Vienna are relatively analogous. The changes in insolation values depending on the measurement point are proportional.
- The graphs for Lisbon are generally steeper and different from the other two locations—i.e., the differences between the lower values (points P1–2A) are smaller between these geographical locations than between the upper values (points 4–5). It also

reflects the measurement of insolation at neutral points for a given geographical location; depending on the other variables, they are almost identical for Oslo (a difference of 62 kWh/m^{2}a (814–876 kWh/m^{2}a)) and Vienna (a difference of 60 kWh/m^{2}a (1057–1117 kWh/m^{2}a)) and higher for Lisbon (a difference of 77 kWh/m^{2}a; 5% (1553–1630 kWh/m^{2}a)).

5. Discussion

The discussion is divided into three parts:

- The first part (Section 5.1) discusses the dependencies between the adopted variables. This provided insight into the importance of each variable in the irradiance of the roof and the relationship between variables.
- In the second part of the discussion (Section 5.2), the collected observations are translated into the electricity yield from the BIPVs in the tested roof configurations. The most and the least favourable tested variants were estimated with a general commentary.
- The last part (Section 5.3) refers to the research limitations.

5.1. Discussion on Dependencies between the Adopted Variables

5.1.1. Geographic Location and Height

The growth of the roof height increases the differences in its irradiation for all locations. These differences are not proportional. Compared with Oslo and Vienna, the increase in roof height in Lisbon is characterised by a more significant difference in irradiation values, as the ranges between the lowest and highest value are larger. This means that the roof's height change in Lisbon is more critical in terms of the occurrence of "favourable" and "unfavourable" roof sections regarding their irradiation. The difference can reach almost 900 kWh/m^{2}a, while for Oslo and Vienna, it reaches a maximum of ≅500 kWh/m^{2}a. In the tested roof orientations, the fields at points P4 and P5 are generally better exposed to sunlight. This applies to all geographies, but the spike is generally the strongest in Lisbon. A relatively constant value characterises differences in irradiation values between Oslo and Vienna. Apart from the apparent fact that Vienna features higher average irradiation than Oslo, the geographical location, in this case, does not affect the different increases or decreases in irradiation because of a shift in the roof height (the corresponding graphs for Oslo and Vienna are relatively parallel).

It can, therefore, be assumed that, in southern countries, with the sun high above the horizon, the height of hypar roofs is more important in terms of their irradiation; in other words, a high canopy causes greater surface limitations in the location of well-sunlit PV cells. The obtained results coincide with the fundamental regularity that, in southern countries, the optimal inclination of solar active planes is closer to the horizontal than in countries at high latitudes, which results from the altitude position of the sun. The second, less obvious observation is that, in these countries, increasing the amplitude of the inclination angles of active solar planes (as in the hypar roof) has a more adverse effect on their irradiation than in northern countries.

5.1.2. Geographic Location, Orientation, and Prestress

In all geographic locations, the relationship between the fields' irradiation values around reference points A and B changes (see Section 5.1.3). In general, these changes are relatively proportional: for example, a change in the azimuth angle (orientation) of the roof causes very similar changes in the insolation of geometries in all three locations. It can be concluded that the geographical location has no noticeable effect on the differences in the "behaviour" of the roof's irradiation under the influence of the orientation rotation. The average irradiation values of roofs indicate this with different orientations and measurements at the neutral point, P3. In detail, the above observation can be applied to prestress 3:1. Considering the results for prestresses 1:1 and 1:3 (for both tested heights), in the tested range of azimuthal angles, with the growth of the angle, the differences in the irradiation values of points on the A-axis increase and decrease on the B-axis. However, only for Lisbon do points 4B and 5B remain the sunniest among the other B-axis areas for all the studied angles. In Oslo and Vienna, at an angle of 45°, the curve of results for B points flattens out or becomes symmetrical to the neutral point, P3, which means that the planes around the B points become similarly irradiated.

The conclusion is that, in southern geographic locations, the distribution of irradiation on a hypar roof depends slightly less on its orientation. These observations can be seen as a part of the general rule that, with the sun higher above the horizon (Lisbon), the orientation of roofs and façades in the context of their irradiation is less important. However, again, the research (see Section 5.1.1) does not confirm the rule that the more to the north a place is situated, the more important it is, because Oslo and Vienna are characterised by a very similar change in roof irradiation behaviour. This observation is quite non-intuitive and requires further research to find the answer as to what latitude the shift in orientation and prestress and the height of hypar roofs starts to have a real significance in the context of their irradiation.

5.1.3. Height and Orientation

The irradiation values of the A and B points diverge with the increase in the azimuthal angle in the examined range of angles. Increasing the height of the roof causes the results to move further apart. This means that the greater the azimuth angle and the bigger the roof height, the greater the differences in the irradiation of individual roof sections. The trends of increase/decrease in the measured values along the A- and B-axes differ. The growth of the azimuthal angle has a more substantial effect on the change in the irradiation value at the A points (the graph becomes steeper). This pitch increases together with the growth of the roof height. In turn, for B points, at a lower elevation, the increase in the azimuth angle causes the graph to flatten out, reaching the horizontal direction, which means that the irradiation values of the B points are closer to each other. However, in the higher of the analysed roofs (H = 3), the graph becomes more and more symmetrical according to the neutral point (P3), so the corresponding opposite points on the B-axis gain similar irradiation values. Generally, therefore, it can be assumed that the planes for points on the B-axis become more neutral in terms of changes in irradiation caused by the increase in the angle, while for those on the A-axis, it is the reverse. In general, considering the average values of irradiation depending on orientation and height, it can be concluded that a change in orientation does not affect the results of the irradiation value, and as already stated, lower roofs are more advantageous.

5.1.4. Prestress and Orientation

The relationship between prestress and orientation is the most complex and irregular. Further detailed descriptions of specific patterns can be found below.

By prestress 1:1, the increase in the azimuth angle (0–45°) causes higher irradiation on the surfaces around the A and B points. However, these differences do not grow very dynamically as in the case of changes in the azimuth angle at constant H (Section 5.1.3). Furthermore, in prestress 1:1, the changes are characterised by regularity, as the graph connecting the irradiation values at individual A and B points changes relatively evenly. In general, the irradiation values of roof sections increase at A points and decrease at B points—similar behaviours, as in the "height–orientation" relationship, evidence similar dependencies. However, smaller differences indicate that the orientation change at a constant prestress (1:1) is less significant regarding roof solar exposure than changing the orientation at a regular height.

By prestresses 1:3 and 3:1, the dependencies are not subject to such clear regularities. The roofs' asymmetric geometries cause the irradiation values measured in the corresponding pairs of points, A and B, to move closer to each other (to P3) and then away from each other (from P3, up). The values diverge the most towards the extreme points (P1A–P1B and P5A and P5B). Therefore, the change in orientation causes the strongest increase in the differences in irradiation recorded at the extreme points, P1 and P5. The irregular distribution of irradiation results from the roof's asymmetric nature. However, this also proves that the change in the irradiation values under the influence of changes in roof orientation is not linear for prestress 3:1.

Similar behaviour can be observed with the reverse geometry, as with prestress 1:3; the graphs of irradiation values are more symmetrical concerning the neutral point, P3, and have a stronger upwards trend towards the extreme point, P5. Thus, the charts are not a mirror image of the 3:1 prestress, which is an important observation. On this basis, it can be assumed that a change in prestress in the downwards direction (e.g., from 1:1 to 1:2) will cause smaller changes in the roof irradiation distribution when changing its orientation than a change in prestress in the upwards direction (e.g., from 1:1 to 2:1) for the tested azimuthal angles.

In general, regardless of the prestress, the change in orientation does not significantly affect the average irradiation of roofs. This means that the relationships described above are significant only when the BIPV is intended to cover only sections of the roof.

5.1.5. Height and Prestress

Height and prestress are the only variables in this study that determine the geometry of the hypar roof. Considering them separately, there is no doubt that a change in their parameters results in a difference in the distribution of insolation. Less obvious are the relationships between these two roof geometrical variables.

Analysing the obtained measurement results at points P1–5, at a height of H = 1, the changes in the irradiation value remain similar for all three tested prestress values; i.e., the graphs do not become more or less steep. This confirms the previous observation that a change in the height of the roof, and not its prestress variable, causes an increase in the differences in the insolation of its individual areas.

Disturbances to the roof symmetry (i.e., a departure from the 1:1 prestress) result in a less regular division into more and less sunlit areas, with these irregularities usually being greater in the case of prestress 3:1. The extreme case is illustrated by the Lisbon variant (azimuth 22.5°, H = 1, prestress 3:1), in which the insolation values at the A points are alternately higher and sometimes lower than the corresponding values at the B points (the graphs intertwine).

With a higher roof height (H = 3), the dynamics of changes in the insolation values remain similar for all three analysed prestress values. This proves that height determines the dynamics of the increase/decrease in the roof's insolation in certain areas. In other words, the contrast between better and worse sunlit parts of the roof does not change significantly under the influence of the prestress variable.

Prestress, on the other hand, changes the relationships between the insolation values in the corresponding pairs of points on the A- and B-axes. This applies mainly to intermediate points (especially the area around P2 in all three azimuth angles tested). This means that the prestress variable can be more strongly "adjusted" to the insolation of the intermediate areas of the hypar roof than to the central and extreme ones.

5.2. Simulation of Energy Gains for Selected Roof Variants

A semi-transparent BIPV roof was adopted for the simulation. It is made of a laminate composed of a transparent coating of ETFE foil and PV cells made of multi-crystalline silicon. The cells are opaque, but their spread within the light-transmitting roof makes it semi-transparent. This is a common way to use BIPVs on membrane roofs [27]. As in these applications, the method of using BIPVs is subject to customisation; simulation calculations were made based on the parameters of a similar product available on the market. Its basic parameters are provided in Table 3, with the nominal power of the module modified assuming the highest currently achieved efficiency of multi-crystalline cells.

Table 3. A semi-transparent PV module was adopted for the simulative calculations (source: elaboration by the authors).

Parameter	Value	Image
Dimension of PV module	72×110 cm (0.792 m^2)	
Nominal power of PV module	96 Wp	
Number of PV cells	28	
Distance between PV cells (vertical and horizontal)	3 cm	
Light transmittance	39%	
Adopted nominal PV power per m^2	121 Wp	
PV cell efficiency (η)	23.3%	

The assumed theoretical electricity yield from solar energy received from the PV system (Psol) was calculated with Formula (1):

$$Psol = Ee * \eta * ef \quad (1)$$

where

Ee = irradiance of a surface (kWh/m^2a);
η = efficiency of the solar cell (%);
ef = PV system efficiency coefficient (%) assumed as 70%.

The calculations considered the extreme and average values of roof irradiation in all tested variants. This allows us to extract the most favourable and least favourable roof variants (five variants each) for two main scenarios:

- A BIPV is used only on a selected section of the roof (the highest/lowest irradiation values around the tested P points; Section 5.2.1).
- The BIPV is assumed to be used on the entire roof surface (average insolation values; Section 5.2.2).

Since it was recognised that the above calculations might not provide a complete picture of the research results, they were supplemented with a ranking of the most favourable and least favourable roofs in terms of the percentage distribution of energy gains. The insolation ranges presented in Figure 8 were used, and solar gains from the PV were calculated on their basis. This ranking can be treated as illustrating an intermediate scenario, for example, when it is not assumed that the entire roof will be covered with PV cells. Also, their use is not limited to the local areas within it (Section 5.2.3).

5.2.1. Recommendations for the Concept of Local BIPV Applications on Hypar Roofs

Calculations of energy yields from PVs, indicated in Table 4, prove that, in the strategy of local BIPV applications on the tested variants of hypar roofs, the most significant benefits are brought about by increasing the roof height from H = 1 to H = 3. Thus, sunlit surfaces are obtained that are best suited for placing PV cells. Regardless of the prestress, it is recommended that the upper convex surface around P5A be oriented perfectly south, i.e., at an azimuthal angle of 45°. The recommendation applies to all location studies. The energy gains that can be achieved (compared with a less favourable location for the PV cells, which reaches approx. 50%). This is important because roofs with H = 3 and an angle of 45° have the least sunny surfaces (around P1A, i.e., the upper convex plane oriented to the north).

For this reason, high roofs should be of particular concern in design decisions regarding local BIPV applications to them. Differences in energy gains calculated in kWh increase with latitude, resulting from a greater increase in the irradiation value in these geographical locations (see Section 5.1.1). The scale of this importance is illustrated by the fact that the measured difference for Lisbon coincides with the unit (m^2) energy demand of a modern office building [41,42] (Table 4).

Table 4. Extreme values indicate the most favourable and least favourable variants regarding solar energy gains from PVs (source: elaboration by the authors).

Model	The Best Variants: Height, Prestress Angle (Points)	Energy from PVs (kWh/m^{2}a)	Model	The Worst Variants: Height, Prestress, Angle (Points)	Energy from PVs (kWh/m^{2}a)
		Oslo			
1	H = 3, 1:1, 45 (P5A)	171.26	1	H = 3, 1:3, 45 (P1A)	85.30
	H = 3, 1:3, 45 (P5A)		2	H = 3, 1:1, 45 (P1A)	85.63
3	H = 3, 3:1, 45 (P5A)	170.28	3	H = 3, 1:3, 22.5 (P1A)	88.40
4	H = 3, 1:3, 22.5 (P5A)	168.32	4	H = 3, 1:1, 22.5 (P1A)	88.56
5	H = 3, 3:1, 22.5 (P5A)	167.50	5	H = 3, 3:1, 22.5 (P1A)	90.68
Maximum difference		85.96 kWh/m^{2}a (50.19% of the highest value)			
		Vienna			
1	H = 3, 3:1, 45 (P5A)	205.02	1	H = 3, 1:3, 45 (P1A)	115.15
2	H = 3, 1:3, 45 (P5A)	204.53	2	H = 3, 1:1, 45 (P1A)	115.64
3	H = 3, 3:1, 22.5 (P5A)	202.24	3	H = 3, 1:3, 22.5 (P1A)	118.57
4	H = 3, 1:3, 45 (P4A)	202.08	4	H = 3, 1:3, 45 (P2A)	124.93
5	H = 3, 1:1, 22.5 (P5A)	201.92	5	H = 3, 3:1, 0 (P1B)	126.57
Maximum difference		89.87 kWh/m^{2}a (43.83% of the highest value)			
		Lisbon			
1	H = 3, 3:1, 45 (P5A)	304.02	1	H = 3, 1:3, 45 (P1A)	160.65
2	H = 3, 1:1, 45 (P5A)	303.86	2	H = 3, 1:1, 45 (P1A)	161.14
3	H = 3, 1:3, 45 (P5A)	303.37	3	H = 3, 1:3, 22.5 (P1A)	173.70
4	H = 3, 1:1, 0 (P5B)	298.96		H = 3, 1:3, 0 (P1B)	
5	H = 3, 3:1, 45 (P5B)	298.64	5	H = 3, 1:1, 22.5 (P1A)	173.86
Maximum difference		143.37 kWh/m^{2}a (47.16% of the highest value)			

5.2.2. Recommendations for the Concept of BIPV Applications to the Entire Surfaces of Hypar Roofs

Calculations of energy yields from PVs are indicated in Table 5, proving that, in the strategy of BIPV application on the entire surfaces of the tested hypar roof variants, the height of the roof is again the most important [43]. However, contrary to the recommendation included in Section 5.2.1, lower roofs (H = 1) are more favourable for BIPVs. In other words, reducing the roof height makes the surfaces more evenly exposed to sunlight, which ultimately brings more benefits than obtaining fragmentary surfaces with the best solar exposure on higher roofs. Changing the prestress, such as changing a 1:1 symmetrical geometry (especially in favour of 3:1), is also beneficial, provided that the roof height is kept low. At higher altitudes (H = 3), changing the prestress, especially to 1:3, has a negative effect. This applies to all surveyed locations.

Recommendations regarding the orientation of the roof are divergent. In the northern location (Oslo), an increase in the azimuthal angle is not conducive to PV energy gains. The angles of 0 and 22.5° are more recommended. This rule is not confirmed in the Central and South European locations. In both locations, among the tested variants, we recommend rotating the roof to an angle of 45°. This rotation allows us to obtain a strongly sunlit surface with a southern orientation, which, in these countries, is more important than the more even roof insolation for the variant in Oslo, which should be a priority for this location (positioning diagonally to the south).

It should be emphasised here that the differences in the energy gains of roofs covered entirely with PV cells are relatively small in the tested variants; i.e., they do not exceed 7% of the highest calculated value of energy gains. Differences in absolute values increase with increasing latitude (as in Section 5.2.1). The difference of 18.07 kWh/m^{2}a measured for Lisbon is not significant for small-area roofs. However, when using a roof with an area of 1000 m^2, with the assumptions made for the simulation under study, the energy gain would amount to 18070 kWh/a, which supplies approx. 120 m^2 of modern (energy-saving) office space [41,42] (Table 5).

Table 5. Average values indicate the most favourable and least favourable variants regarding solar energy gains from PV (source: elaboration by the authors).

Model	The Best Variants: Height, Prestress Angle	Energy from PVs (kWh/m^{2}a)	Model	The Worst Variants: Height, Prestress, Angle	Energy from PVs (kWh/m^{2}a)
		Oslo			
1	H = 1, 3:1, 0	141.63	1	H = 3, 1:3, 45	132.20
2	H = 1, 3:1, 22.5 H = 1, 3:1, 0	141.62	2 3	H = 3, 1:3, 22.5 H = 3, 1:3, 0	132.25 132.33
4	H = 1, 1:3, 0	141.22	4	H = 3, 3:1, 0	135.26
5	H = 1, 1:3, 22.5	141.22	5.	H = 3, 3:1, 22.5	135.27
Maximum difference		9.43 kWh/m^{2}a (6.66% of the highest value)			
		Vienna			
1	H = 1, 3:1, 45	180.61	1	H = 3, 1:3, 0	168.04
2	H = 1, 3:1, 22.5	180.60	2	H = 3, 1:3, 22.5	168.07
3	H = 1, 3:1, 0	180.58	3	H = 3, 1:3, 45	168.08
4	H = 1, 1:3, 22.5 H = 1, 1:3, 45	180.15	4	H = 3, 3:1, 0	171.09
5	H = 1, 1:3, 0	180.14	5	H = 3, 3:1, 22.5	171.34
Maximum difference		12.57 kWh/m^{2}a (6.96% of the highest value)			
		Lisbon			
1	H = 1, 3:1, 45	263.84	1	H = 3, 1:3, 0	245.77
2	H = 1, 3:1, 22.5	263.80	2	H = 3, 1:3, 22.5	245.79
3	H = 1, 3:1, 0	263.68	3	H = 3, 1:3, 45	245.88
4	H = 1, 1:3, 22.5 H = 1, 1:3, 45	262.96	4	H = 3, 3:1, 0	250.82
5	H = 1, 1:3, 0	262.95	5	H = 3, 1:1, 0	251.61
Maximum difference		18.07 kWh/m^{2}a (6.85% of the highest value)			

5.2.3. Recommendations for the Strategy of Partial Roofing with PV Cells (Intermediate Scenario between Local and Entire BIPV Roof Coverage)

In a way, the additional ranking sheds entirely new light on the previous recommendations in Sections 5.2.1 and 5.2.2. Although this confirms the priority importance of the roof height in energy gains from PVs, it does not, as in the previous points, indicate a more favourable height that would be universal for all surveyed geographic locations. The percentage distribution of the expected energy gains clearly shows that a lower roof height, as in the case of the BIPV total roofing strategy, can only be recommended for Oslo and Lisbon. In these locations, at a height of H = 1, the highest share of areas is observed where BIPV profits may exceed 130 kWh/m^2 and 261 kWh/m^2, respectively (these values were calculated from the insolation values contained in Figure 8 and based on Formula (1)). In these locations, the best results are obtained with a prestress of 3:1 and the worst are obtained with a prestress of 1:3. In the discussed strategy, the choice of height and, to a lesser extent, prestress is more critical for Oslo than for Lisbon. In a northern location, you can gain almost 45% "better" energy-wise space, while in Lisbon, less than 24%. The adopted ranges of solar gains are conventional. They serve to develop general views by illustrating the tendencies of changes in the "energy distribution" of the roof under the influence of the examined variables.

Vienna breaks out of the above regularities. It should be recalled that Vienna is a location where insolation distributions were recorded in as many as three adopted ranges (Figure 8), which were converted into three values of energy gains from PVs. For this reason, selecting the least favourable variants can be assessed according to two different criteria: the largest percentage of the area in the lowest insolation range or the total share in the two lowest ranges. The second criterion was adopted because higher shares of areas with the highest gains accompanied variants with a high share of areas with the lowest solar gains. Therefore, adopting the first criterion would provide a distorted picture. Thus, according to the adopted second criterion, it can be concluded that, for Vienna, not H = 1 but H = 3 should be recommended for the discussed scenario of indirect BIPV application. How can this breach be explained?

Given that this recommendation is the same as the recommendation for the local BIPV application scenario (Section 5.2.1), it can be assumed that the local roof spots with the high energy gains measured for Vienna are more extensive than in the roofs in the northern and southern locations. This is confirmed by the lowest percentage difference for Vienna between the local places with the highest and lowest energy gains. The difference in prestress is also noteworthy. Unlike Oslo and Lisbon, a prestress of 1:3 should be recommended for the discussed location. Vienna, representing the Central European location, confirms that the issue of obtaining solar energy is particularly complex, as it oscillates between dominant solar gains from the horizontal and vertical directions. This aspect requires further research (Table 6).

Table 6. The most and least favourable variants regarding the percentage distribution of the best and worst areas in terms of the number of solar gains from PV energy gains (source: elaboration by the authors).

Oslo

Model	The Best Variants: Height, Prestress Angle	Energy from PV (kWh/m^2a)		Model	The Worst Variants: Height, Prestress, Angle	Energy from PVs (kWh/m^2a)	
		>130	<130			>130	<130
1	H = 1, 3:1, 45	98.27	1.73	1	H = 3, 1:3, 22.5	53.53	46.47
2	H = 1, 3:1, 22.5	97.94	2.06	2	H = 3, 1:3, 45	53.54	46.46
3	H = 1, 1:1, 22.5	90.53	9.47	3	H = 3, 1:3, 0	53.91	46.09
4	H = 1, 1:1, 45	90.19	9.81	4	H = 3, 3:1, 0	58.67	41.33
5	H = 1, 1:1, 0	90.12	9.88	5	H = 3, 1:1, 45	58.70	41.30
Maximum difference			9.43 kWh/m^2a (6.66% of the highest value)				

Vienna

Model	The Best Variants: Height, Prestress Angle	Energy from PV (kWh/m^2a)		Model	The Worst Variants: Height, Prestress, Angle	Energy from PVs (kWh/m^2a)	
		>195	<195			>195 (>130)	<195
1	H = 3, 1:3, 45	29.06	70.94	1	H = 1, 1:1, 22.5	100 (99.62)	0
2	H = 3, 1:3, 22.5	27.34	62.66		H = 1, 1:1, 22.5		
3	H = 3, 3:1, 0	12.56	87.44	2	H = 1, 1:3, 0	100 (0)	0
4	H = 3, 1:1, 22.5	6.65	93.35		H = 1 3:1, 0		
5	H = 3, 1:3, 0	6.35	93.65	5	H = 1, 3:1, 22.5	99.97 (0)	0.03
Maximum difference			70.94% of the roof area				

Lisbon

Model	The best variants: height, prestress angle	Energy from PV (kWh/m^2a)		Model	The worst variants: height, prestress, angle	Energy from PV (kWh/m^2a)	
		>260	<260			>260	<260
1	H = 1, 3:1, 45	60.27	39.73	1	H = 3, 3:1, 45	36.89	63.11
2	H = 1, 1:1, 45	58.22	41.78	2	H = 3, 1:3, 0	43.22	56.78
3	H = 1, 1:1, 0	57.94	42.06	3	H = 3, 1:3, 22.5	44.69	55.31
4	H = 1, 1:1, 22.5	57.89	42.11	4	H = 3, 1:1, 45	44.94	55.06
5	H = 1, 3:1, 22.5	57.42	42.48	5	H = 3, 1:1, 0	46.82	53.18
Maximum difference			23.38% of the roof area				

5.3. Research Limitations

The results of this research should be treated as helpful in understanding the importance of geographical location and changes in the orientation and geometry of hypar roofs for the use of solar energy. These are illustrative results that may be helpful for designers, especially in the conceptual phase when making decisions regarding the variables under study. They are also helpful for designing roofs in different latitudes in terms of optimising the use of BIPVs. To systematise the research and limit the number of tested variants, the authors had to limit the number of variables at the same time, which is a significant research limitation. Further research, e.g., in relation to one variable (e.g., height or prestress) but with a larger number of values, would allow for more detailed observations, e.g., to determine whether changes in the roof insolation value are linear or geometric. Restricting to three azimuthal angles is a representative test "sample". Given the symmetry of the model, some of the azimuthal angles are a mirror image of the adopted values. This means that the results would be the same for angles of 0, 90, 180, and 270°. Likewise, the results are the same for angle values of 45, 135, 225, and 315°. For a value of 22.5°, identical results are obtained for angles of 67.5, 112.5, 157.5, 202.5, 247.5, 292.5, and 337.5°. Therefore, practically, the research provides results for 16 different orientation angles of the structure. The three geographic locations selected left an unanswered question, which was framed in terms of conjecture, not evidence. It has not been proven where the similarities between the extreme locations (Oslo and Lisbon) and the difference in Vienna in terms of recommendations for the strategy of partial roofing with PV cells (Section 5.2.3) come from. Exploring more intermediate geographic locations would help answer this question.

Another limitation is the number of measurement points on the roof. Their limited number provides a general view of changes in the insolation of the roof surface but cannot determine with greater accuracy what the differences in insolation look like in intermediate places. Extensive research is possible for individual solutions and should be conducted after identifying the pros and cons that the results of this study provide.

Finally, this research was limited to one type of PV cell. The PV system efficiency coefficient was assumed to be 70%. Detailed research, limited even to one type of PV cell, requires the adoption of a larger number of variables that potentially and additionally affect the energy obtained from the PV system: among others, the temperature of the external and internal surface of the roof with PV cells; the method of connecting the cells (serial or parallel); and the technical parameters of other components of the PV system (e.g., cabling and inverters). In this study, in order to achieve its goal, such detailed assumptions were treated as redundant and, in some aspects, additionally difficult to take into account (e.g., calculating the roof temperature in each of its sections).

This research relates to the energy optimisation of PV integration with hypar roofs. Energy gains translate directly into financial savings related to the use of the building, which is an undoubted incentive to search for optimisation. An economic analysis goes beyond the scope of this research, but it is advisable to undertake it as part of separate research.

6. Conclusions

The optimal position of photovoltaic cells in terms of energy gains related to exposure to solar radiation was investigated for hypar roof geometries. Simulations were performed for 54 roof samples with the following geometric variables: roof height (1.0, 3.0 m) and prestress (1:3, 1:1, 3:1). The research was conducted for three roof orientations defined by azimuth angles of 0, 22.5, and 45 degrees and three geographic locations, Oslo, Vienna and Lisbon, representing Northern, Central and Southern Europe, respectively. The Sofistik and Rhino + Ladybug software were used to create models and simulations. The study confirmed that hypar roofs have complex geometries that are difficult to assess in terms of the optimal use of BIPVs without simulating the irradiation of their surfaces.

This fact justified the need for this study. The obtained results proved the need for the well-thought-out use of BIPV knowledge regarding the influence of geometrical variables and azimuth on roof insolation. The incorrect positioning of PV cells can lead to energy losses of up to 50%.

The obtained results indicate the primary role of roof curvature as a factor determining irradiation conditions and, consequently, energy gains from BIPVs. In general, fewer curved roofs are preferable. The prestress and azimuth angle are of lesser, but noticeable, importance, although it is difficult to provide an unambiguous general assessment of the best solutions here, detailed assessments are included in the discussion above.

From the beginning, it was obvious that the greatest energy gains could be expected in the southern location (Lisbon) and the smallest in the northern location (Oslo). The research confirmed this, but at the same time, it showed that changes in irradiation under the influence of the studied variables are not proportional in these locations. This means that it is not possible to draw conclusions about the results for another location based on the result obtained for one location. This indicates the need for an individual, different approach to the design of hypar roofs at different latitudes. Despite large differences between the irradiation of roofs for Oslo and Lisbon, up to twice the results, a poorly designed BIPV roof in Lisbon can deliver less PV electricity than an optimised BIPV roof in Oslo (although this is the extreme case and applies to point applications). This proves the usefulness of this type of research.

The recommendations included in the Discussion section revealed one more important conclusion. Defining the optimal use of a BIPV depends on the adopted scenario regarding the coverage percentage. Other recommendations concern the strategy of entire roof coverage with PV cells and others, such as local or partial (as described in Sections 5.2.1–5.2.3). This conclusion may be particularly important for designers in the early design phase and contribute to finding solutions that will optimise the proportions between investment outlays on PVs and energy gains that can be derived from them.

Author Contributions: Conceptualisation, J.M.; methodology, J.M., V.M. and E.L.; software, A.S.; validation, J.M., V.M., A.S. and E.L.; formal analysis, J.M., V.M., A.S. and E.L; investigation, J.M., V.M., A.S. and E.L.; data curation, J.M., V.M., A.S. and E.L.; writing—original draft preparation, J.M., V.M., A.S. and E.L.; writing—review and editing, J.M., V.M. and E.L.; visualisation, J.M. and A.S.; supervision, J.M. project administration, J.M. and E.L.; funding acquisition, E.L. All authors have read and agreed to the published version of the manuscript.

Funding: This research received no external funding.

Data Availability Statement: Not applicable.

Conflicts of Interest: The authors declare no conflict of interest.

References

1. European Parliament. Directive 2018/2001 of the European Parliament and of the Council of 11 December 2018 on the Promotion of the Use of Energy from Renewable Sources. 2018. Available online: https://eur-lex.europa.eu/legal-content/EN/TXT/?uri=uriserv:OJ.L_.2018.328.01.0082.01.ENG (accessed on 13 July 2023).
2. Renewable Energy Policy Network for the 21st Century (REN21). *Renewables 2019 Global Status Report-REN21*; Secretariat: Paris, France, 2019.
3. European Parliament. Directive 2010/31/EU of the European Parliament and of the Council of 19 May 2010 on the energy performance of buildings. *J. Eur. Union* **2010**, *153*, 13–35. Available online: https://eur-lex.europa.eu/legal-content/EN/ALL/;ELX_SESSIONID=FZMjThLLzfxmmMCQGp2Y1s2d3TjwtD8QS3pqdkhXZbwqGwlgY9KN!2064651424?uri=CELEX:32010L0031 (accessed on 13 July 2023).
4. European Parliament. Directive 2012/27/EU of the European Parliament and of the Council of 25 October 2012 on energy efficiency. *J. Eur. Union* **2012**, *315*, 1–56.
5. European Parliament. Directive 2009/28/EC of the European Parliament and of the Council of 23 April 2009 on the Promotion of the Use of Energy from Renewable Sources. 2009. Available online: https://eur-lex.europa.eu/legal-content/EN/TXT/PDF/?uri=CELEX:32009L0028 (accessed on 13 July 2023).
6. Lucchi, E. Renewable Energies and Architectural Heritage: Advanced Solutions and Future Perspectives. *Buildings* **2023**, *13*, 631. [CrossRef]
7. Baltas, A.E.; Dervos, A.N. Special framework for the spatial planning & the sustainable development of renewable energy sources. *Renew. Energy* **2012**, *48*, 358–363.

8. Lucchi, E.; Adami, J.; Peluchetti, A.; Mahecha Zambrano, J.C. Photovoltaic potential estimation of natural and architectural sensitive land areas to balance heritage protection and energy production. *Energy Build.* **2023**, *290*, 11310. [CrossRef]
9. IEA-SHC T41. Solar Energy and Architecture. Available online: http://task41.iea-shc.org (accessed on 13 July 2023).
10. Lucchi, E. Integration between photovoltaic systems and cultural heritage: A socio-technical comparison of international policies, design criteria, applications, and innovation developments. *Energy Policy* **2022**, *171*, 112203. [CrossRef]
11. Lucchi, E.; Baiani, S.; Altamura, P. Design criteria for the integration of active solar technologies in the historic built environment: Taxonomy of international recommendations. *Energy Build.* **2023**, *278*, 112651. [CrossRef]
12. Otto Muller, M.; Stämpfli, A.; Dold, U.; Hammer, T. Energy autarky: A conceptual framework for sustainable regional development. *Energy Policy* **2011**, *39*, 5800–5810.
13. *EN 50583-1*; Photovoltaics in buildings—Part 1: BIPV Modules. Comité Européen de Normalisation Electrotechnique (CENELEC): Bruxelles, Belgium, 2016.
14. Berger, K.; Cueli, A.B.; Boddaert, S.; Del Buono, S.; Delisle, V.; Fedorova, A. International definitions of "BIPV", Report IEA-PVPS T15-04: 2018. Available online: https://iea-pvps.org/wp-content/uploads/2020/02/IEA-PVPS_Task_15_Report_C0_International_definitions_of_BIPV_hrw_180823.pdf (accessed on 13 July 2023).
15. *IEC TS 61836:2016*; Solar Photovoltaic Energy Systems. Terms, DEFINITIONS and Symbols. International Electrotechnical Commission (IEC): Bruxelles, Belgium, 2016.
16. *IEC 61730-1*; Photovoltaic (PV) Module Safety Qualification. Part 1: Requirements for Construction. International Electrotechnical Commission (IEC): Bruxelles, Belgium, 2016.
17. Chang, R.; Cao, Y.; Lu, Y.; Shabunko, V. Should BIPV technologies be empowered by innovation policy mix to facilitate energy transitions?-Revealing stakeholders' different perspectives using Q methodology. *Energy Policy* **2019**, *129*, 307–318. [CrossRef]
18. Inayatullah, J.; Waheed, U.; Muhammad, A. Social acceptability of solar photovoltaic system in Pakistan: Key determinants and policy implications. *J. Clean. Prod.* **2020**, *274*, 123140.
19. Kumar Shukla, A.; Sudhakar, K.; Baredar, P.; Mamat, R. Solar PV and BIPV system: Barrier, challenges and policy recommendation in India. *Renew. Sustain. Energy Rev.* **2018**, *82*, 3314–3322. [CrossRef]
20. Yuan, X.; Zuo, J.; Ma, C. Social acceptance of solar energy technologies in China. End users' perspective. *Energy Policy* **2011**, *39*, 1031–1036. [CrossRef]
21. Lucchi, E.; Dall, I.; Peluchetti, A.; Toledo, L.; Pelle, M.; López, C.P.; Guazzi, G. Photovoltaic technologies in historic buildings and protected areas: Comprehensive legislative framework in Italy and Switzerland. *Energy Policy* **2022**, *116*, 112772. [CrossRef]
22. Lim, C.H.; Kamaruzzaman, S.; Yusof, S. Public response to residential building integrated photovoltaic system (BIPV) in Kuala Lumpur urban area. In Proceedings of the 4th IASME/WSEAS International Conference on Energy & Environment, Cambridge, UK, 24–26 February 2019.
23. Cohen, J.J.; Reichl, J.; Schmidthaler, M. Re-focussing research efforts on the public acceptance of energy infrastructure: A critical review. *Energy* **2014**, *76*, 4–9. [CrossRef]
24. Li, Q.; Zanelli, A. A review on fabrication and applications of textile envelope integrated flexible photovoltaic systems. *Renew. Sustain. Energy Rev.* **2021**, *139*, 110678. [CrossRef]
25. Zhang, J.; Zhang, W.; Cheng, H.-M.; Silva, S.R.P. Critical review of recent progress of flexible perovskite solar cells. *Mater. Today* **2020**, *39*, 66–88. [CrossRef]
26. Green, M.A. Third generation photovoltaics: Solar cells for 2020 and beyond. *Phys. E* **2002**, *14*, 65–70. [CrossRef]
27. Milošević, V.; Marchwiński, J. Photovoltaic Technology Integration with Tensile Membrane Structures: A Critical Review. *Tech. Gaz.* **2022**, *29*, 702–713.
28. Kibria, M.T.; Ahammed, A.; Sony, S.M.; Hossain, F.; Shams, U.I. A Review: Comparative studies on different generation solar cells technology. In Proceedings of the 5th International Conference on Environmental Aspects of Bangladesh, Dhaka, Bangladesh, 6–8 March 2015; pp. 51–53.
29. Mullasery, D.J. *Perovskite Solar Cells Degradation Solutions*; Technical Report, 637-645; University of British Columbia: Vancouver, BC, Canada, 2016.
30. Borazan, I.; Bedeloglu, A.C.; Demir, A. A photovoltaic textile design with a stainless steel mesh fabric. *J. Ind. Text.* **2022**, *51*, 1527–1538. [CrossRef]
31. Zanelli, A.; Monticelli, C.; Beccarelli, P.; Ibrahim, H. Experimental manufacture of a pneumatic cushion made of ETFE foils and OPV cells. In *Textiles Composites and Inflatable Structures V, Proceedings of the V International Conference on Textile Composites and Inflatable Structures, Barcelona, Spain, 5–7 October 2011*; CIMNE: Barcelona, Spain, 2011; pp. 279–290.
32. Ibrahim, H.; Wagdy, A.; Beccarelli, P.; Carpenter, R.; Chilton, J. Applicability of flexible photovoltaic modules onto membrane structures using grasshopper integrative model. *Procedia Eng.* **2016**, *155*, 379–387. [CrossRef]
33. Zhang, J.; Yang, Q.; Li, B. Form-state and loading analyses of air-flated cushion membrane structures. *J. Harbin Inst. Technol.* **2008**, *40*, 1569–1572.
34. Zhao, B.; Hu, J.; Chen, W.; Chen, J.; Jing, Z. Dynamic geometrical shape measurement and structural analysis of inflatable membrane structures using a low-cost three camera system. *Autom. Constrution* **2018**, *96*, 442–456. [CrossRef]
35. Schek, H.J. The force density method for form finding and computation of general networks. *Comput. Methods Appl. Mech. Eng.* **1974**, *3*, 115–134. [CrossRef]

36. Gosling, P.D.; Bridgens, B.N.; Albrecht, A.; Alpermann, H.; Angeleri, A.; Barnes, M.; Bartle, N.; Canobbio, R.; Dieringer, F.; Gellin, S.; et al. Analysis and Design of Membrane Structures: Results of a Round Robin Exercise. *Eng. Struct.* **2013**, *48*, 313–328. [CrossRef]
37. Milošević, V.; Marković, B. Comparison of point and snow load deflections in design and analysis of tensile membrane structures. *Adv. Civ. Eng.* **2020**, *2020*, 8810085. [CrossRef]
38. Humm, O.; Toggweiler, P. *Photvoltaics in Architecture*; Birkhäuser Verlag: Basel, Switzerland, 1991; p. 97.
39. Software Sofistik. Available online: https://www.sofistik.de (accessed on 13 July 2023).
40. Ladybug Grasshopper Analysis Software. Available online: www.ladybug.tools/epwmap/ (accessed on 13 July 2023).
41. Jak Obliczyć Uzysk Energii z Instalacji Fotowoltaicznej. Available online: https://www.kompaniasolarna.pl/fotowoltaika/obliczyc-uzysk-energii-instalacji-fotowoltaicznej/ (accessed on 30 June 2023).
42. Saleem, M. Energy Benchmarking—How Much Energy Usage is Normal for Your Building? Available online: https://clevair.io/en/blog/energy-benchmarking-buildings (accessed on 13 July 2023).
43. Zużycie energii w budynkach biurowych (The Energy Use in Office Buildings)—Raport. Available online: https://www.skanska.pl/4a2b98/siteassets/oferta/biura/raporty-i-standardy/raport-zuycia-energii-w-budynkach-biurowych/zuzycie-energii-w-budynkach-biurowych-raport.pdf (accessed on 2 July 2023).